

RESEARCH

Open Access



Microstructure reconstruction and structural equation modeling for computational design of nanodielectrics

Yichi Zhang¹, He Zhao¹, Irene Hassinger², L. Catherine Brinson¹, Linda S. Schadler² and Wei Chen^{1*}

* Correspondence:
weichen@northwestern.edu
¹Northwestern University, Evanston,
USA
Full list of author information is
available at the end of the article

Abstract

Nanodielectric materials, consisting of nanoparticle-filled polymers, have the potential to become the dielectrics of the future. Although computational design approaches have been proposed for optimizing microstructure, they need to be tailored to suit the special features of nanodielectrics such as low volume fraction, local aggregation, and irregularly shaped large clusters. Furthermore, key independent structural features need to be identified as design variables. To represent the microstructure in a physically meaningful way, we implement a descriptor-based characterization and reconstruction algorithm and propose a new decomposition and reassembly strategy to improve the reconstruction accuracy for microstructures with low volume fraction and uneven distribution of aggregates. In addition, a touching cell splitting algorithm is employed to handle irregularly shaped clusters. To identify key nanodielectric material design variables, we propose a Structural Equation Modeling approach to identify significant microstructure descriptors with the least dependency. The method addresses descriptor redundancy in the existing approach and provides insight into the underlying latent factors for categorizing microstructure. Four descriptors, i.e., volume fraction, cluster size, nearest neighbor distance, and cluster roundness, are identified as important based on the microstructure correlation functions (CF) derived from images. The sufficiency of these four key descriptors is validated through confirmation of the reconstructed images and simulated material properties of the epoxy-nanosilica system. Among the four key descriptors, volume fraction and cluster size are dominant in determining the dielectric constant and dielectric loss.

Keywords: Nanodielectric, Material design, Descriptor identification, Microstructure characterization and reconstruction, Structural Equation Modeling

Background

Dielectric materials are widely used in mobile electronics, electrical transmission, and pulsed power applications [1]. There is an increasing demand for new nanodielectric materials, consisting of nanoparticle-filled polymers, for creating future electrical transmission and storage devices. One example is a new capacitor made from nanodielectrics that can store a large amount of energy and discharge it quickly with high-energy density [2]. The design of nanodielectrics is often multi-objective, for example, a tradeoff between dielectric constant and breakdown strength of dielectric materials

has been observed [3]. It has been noted that small volume fractions of nanofillers can significantly improve the composites' dielectric breakdown strength because of their high surface area/internal volume ratio [4]. To achieve design requirements under different application scenarios, a systematic computational design approach is needed to quickly explore the microstructure design space of nanodielectrics. In this work, we are developing characterization, reconstruction, and key microstructure feature identification techniques to support the computational design of nanodielectric systems.

A traditional material design follows a trial-and-error process with the focus on exploring the relationships between processing conditions and material properties. This empirical approach to material design is expensive and time consuming. In integrated computational materials engineering (ICME), a three-link (i.e., processing-structure-property) chain model that enables "microstructure-mediated design" has been proposed to facilitate the design of new materials [5, 6]. The microstructure material design problem can be formulated as an optimization problem, in which the desired material properties drive the design of microstructure first and then the corresponding processing conditions. As pointed out by Xu et al, ICME faces three design-related challenges: *design representation*, *design evaluation*, and *design optimization* [7]. *Design representation* requires quantitative representation of the design space of heterogeneous microstructures using a small set of design variables. *Design evaluation* is the process of assessing material properties for a given microstructure morphology, which often involves finite element modeling (FEM) and simulations. *Design optimization* searches for the optimal microstructure design to achieve the desired material properties. Using the design of nanodielectrics as a focal application, the main focus of this paper is on developing methods to support design representation and identify key microstructural design variables in material design.

A good design representation means an accurate quantitative description of microstructures that is easy to control from the perspective of simulation, design, and processing. In the existing work, methods have been developed to characterize and reconstruct microstructures for different material systems. They can be mainly classified into two categories: one is to use correlation functions (CFs) such as 2-point CF, 2-point cluster CF, and surface correlation [8–11]; the other is to use *physical descriptors*, such as volume fraction, particle size, and minimum distance between particles [12]. CF-based reconstruction often involves optimization procedures to minimize the error between the actual CF and the target ones. This approach has been extended for reconstructing multiphase microstructures, for which each phase has its own CF [13, 14]. Although CF-based approaches are flexible and can be adapted for different microstructures, it is computationally expensive and prohibitive for use as a part of the iterative material design procedure. In addition, CFs are infinitely dimensional. While coefficients of the functions can be treated as design variables, they lack physical meaning. The descriptor-based approach, on the other hand, is much more intuitive and offers low dimensionality of design variables with clear physical meaning. Toward this end, Xu et. al. [12, 15] proposed a descriptor-based approach to fully characterize particle-based microstructures by introducing three categories of descriptors: (1) *composition*: e.g., volume fraction; (2) *dispersion*: e.g., nearest center distance, interphase area, cluster number, local volume fraction, and orientation; (3) *geometry*: e.g., cluster area, equivalent radius, aspect ratio, eccentricity, roundness, compactness, tortuosity, pore size, and rectangularity.

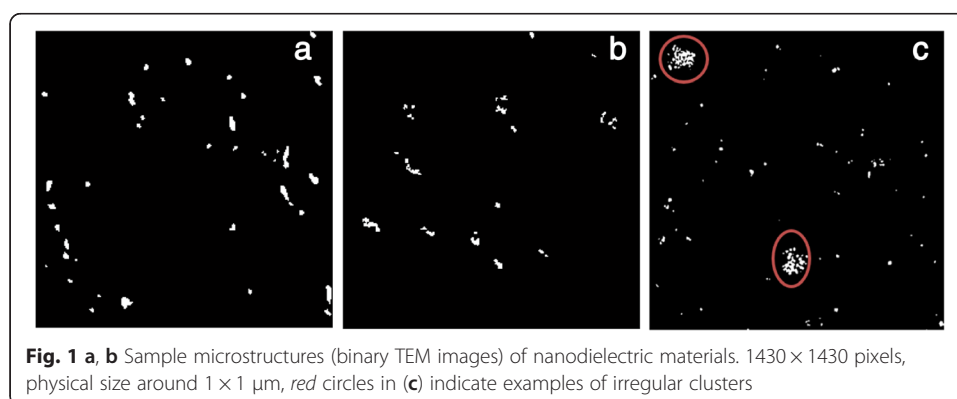
A descriptor-based approach is more efficient for generating statistically equivalent microstructures than the CF-based approach and has been found effective for polymer nanocomposites that have a relatively high volume fraction of filler (e.g., over 20 %) [7, 12]. In this work, the nanodielectric system of interest has a few special features (shown in Fig. 1):

- Low volume fraction and small number of clusters
- Uneven distribution of aggregates (heterogeneity)
- Irregularly shaped large clusters that cannot be modeled using simple geometries like a sphere or ellipse (see Fig. 1c)

The volume fraction of the nanodielectric fillers ranges from 0.5 to 3 % over the samples available in our study (collected from several dielectric systems with similar polymer dielectric permittivity). When the filler phase is on the nanoscale, small filler loadings can result in significant property improvement because of the large interfacial area. When the volume fraction is high, aggregation is harder to control and the property enhancements are reduced. As a consequence, the distribution is heterogeneous after processing, which is the reason why, as shown in Fig. 1c, local aggregates (marked by circles) can be observed in these microstructures. In addition, the dispersion (ability to separate primary particles) depends on the particle/particle and particle/polymer attraction [16]. The greater the particle/polymer enthalpic incompatibility, the greater the driving force for agglomeration.

While the descriptor-based method is generally applicable for particle-based nanodielectrics, the original reconstruction algorithm requires the microstructures to be simple and the distribution of filler phase to be even, which is not always satisfied in low volume fraction nanodielectric systems. Therefore, the existing descriptor-based method needs to be tailored to suit the special features of nanodielectrics.

Material informatics [17, 18] is a growing area that exploits information technology and data science to represent, manage, and analyze material data for accelerating new material discovery and design. One of the common challenges associated with material informatics is the high dimensionality of the data and the design space. Recently, efforts have been made in microstructure dimensionality reduction via manifold learning [19] and principal components [20]. However, dimension reduction based only on microstructures does not reflect the influence of microstructure on the properties of interest.



To address such limitations, our recent work applied a supervised learning algorithm by using structural information from images and material properties from simulations [21] as supervisory (response) signals. Even though the method can determine the relative importance of descriptors, it introduces subjectivity when determining the final set of design variables. In addition, this learning method is not capable of discriminating redundant features (descriptors); neither it is reliable for cases with a small number of sample images.

In this work, we employ the descriptor-based characterization and reconstruction method to the particular nanodielectric system of interest. To achieve more realistic characterization and more accurate reconstruction, the existing algorithms are modified considering the aforementioned special features of the nanodielectric system. To address the issue of irregularly shaped large clusters, a touching cell splitting algorithm [22] is incorporated to reproduce more realistic structures. To capture the unevenly distributed aggregates, we propose a decomposition and reassembly strategy for reconstruction that preserves local microstructural information. To overcome the limitations of the existing machine learning approach, a Structural Equation Modeling [23] approach is proposed in this work to choose the proper set of independent descriptors using the information learned from images. By introducing latent layers in mapping input and output relations, we are able to identify the relationships and dependencies among descriptors, which allow determination of a small set of key descriptors as design variables. Finally, we illustrate the obtained relationship between key microstructural descriptors and the dielectric properties to support design of a nanoscale silica/epoxy matrix system.

Methods

Descriptor-based characterization and reconstruction

With various microscopic imaging techniques, such as scanning electron microscopy [24] and transmission electron microscopy (TEM) [25], material microstructures can be represented by grayscale digital images. Descriptor characterization is a process for extracting statistical information about the structure descriptors from the images. Due to the heterogeneity of these microstructures, statistical moments are often used as a part of the descriptors. For instance, “cluster area” as a descriptor is best described by a statistical distribution rather than a single value. To reduce dimensionality in representation, the first several orders of statistical moments, such as mean and variance are often used rather than considering the whole distribution.

Once a microstructure is characterized by descriptors, a typical 2D or 3D reconstruction follows a sequential procedure [12]: (1) *dispersion reconstruction*: center positions of clusters are adjusted to match dispersion descriptors, e.g., the nearest center distances, using optimization algorithms such as simulated annealing (SA), (2) *geometry reconstruction*: the geometry is randomly generated for each cluster based on the geometry descriptors and geometry profiles are assigned to each cluster, (3) *composition adjustment*: the edge of clusters are modified to satisfy the composition descriptors such as the volume fraction.

Because the primary particle size is small in this system, noise in the grayscale TEM images is more likely to be recognized as particles in image processing. In this work, we first employ Gaussian filtering [26] to remove the influence of noise. Gaussian

filtering utilizes a Gaussian kernel to smooth the image, which will remove isolated pixels. After the filtering process, the existing descriptor-based characterization and reconstruction algorithm as described earlier is employed.

Touching cell splitting method

In the existing descriptor-based characterization [7], all connected regions are considered clusters and are approximated by ellipses. However, for the nanodielectric system in our study, it is observed that the shapes of many connected regions are irregular, which introduces inaccuracy when using a simple ellipse approximation as shown in Fig. 2b.

To improve the characterization accuracy, a touching cell splitting algorithm [22] is applied to split large irregular clusters. The algorithm uses polygon approximation and ellipse fitting techniques to achieve the goal of separation. One simple example is shown in Fig. 3b, where one large cluster is split into three ellipses. To achieve this, the splitting algorithm follows three basic steps:

- 1) Polygon approximation of cluster edges
- 2) Identification of concave points and segmentation of cluster edges
- 3) Separation with ellipse fitting

A polygon approximation pre-process is first applied, to avoid the evaluation of concavity of each point on the edge of aggregates. This first step is beneficial for reducing the noise on the contour of aggregates as well as reducing the computational time, which is proportional to the number of points to be evaluated. As shown in Fig. 3a, after the polygon approximation using an octagon, the contour can be simply represented by a sequence of points (marked by blue dots), and the concavity at each location can be easily approximated by the angle difference between the neighbors:

$$\begin{aligned} a(P_{\text{pre}}, P_c) &= \tan^{-1} \left((y_{\text{pre}} - y_c) / (x_{\text{pre}} - x_c) \right), \\ a(P_{\text{next}}, P_c) &= \tan^{-1} \left((y_{\text{next}} - y_c) / (x_{\text{next}} - x_c) \right) \end{aligned} \quad (1)$$

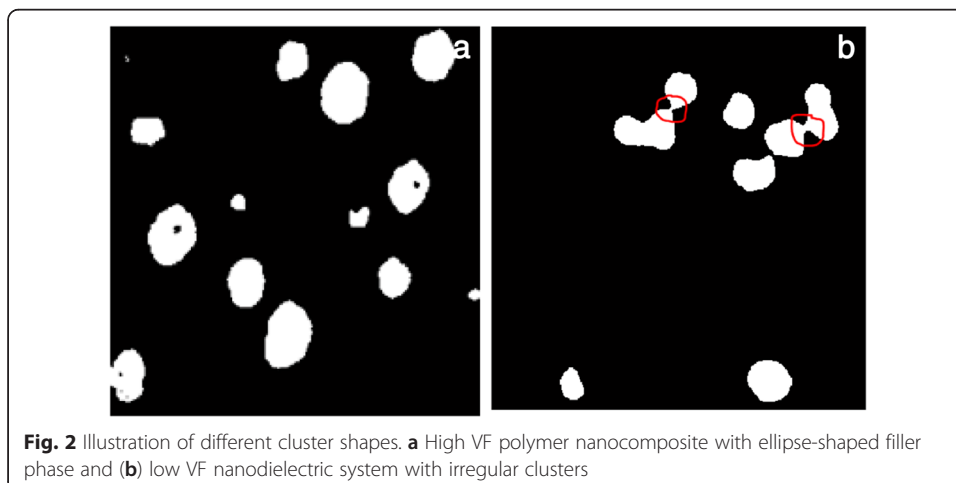
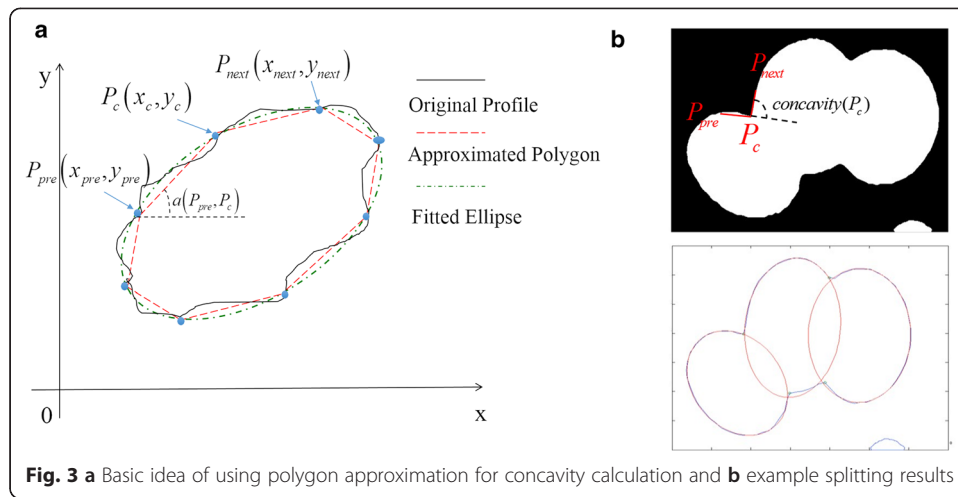


Fig. 2 Illustration of different cluster shapes. **a** High VF polymer nanocomposite with ellipse-shaped filler phase and **(b)** low VF nanodielectric system with irregular clusters



$$\text{concavity}(P_c) = \begin{cases} |a(P_{pre}, P_c) - a(P_{next}, P_c)|, & \text{if } |a(P_{pre}, P_c)| < \pi, \\ \pi |a(P_{pre}, P_c) - a(P_{next}, P_c)|, & \text{else} \end{cases} \quad (2)$$

where P_c is the location to be evaluated and P_{pre}, P_{next} are the neighbor points next to it. Real concave points should satisfy the following rules:

- 1) $\text{concavity}(P_c) \in (a_1, a_2)$, and
- 2) Line $\overline{P_{pre}P_{next}}$ should not cross over the inner region of the aggregates.

The first rule indicates that a proper threshold interval of concavity needs to be set to select the candidates of real concave points. The choice of the interval varies for different material systems. Once the concave points are identified, the entire contour of aggregates can be represented by several segments to fit ellipses. To represent the ellipses, an implicit second order polynomial is utilized, i.e.:

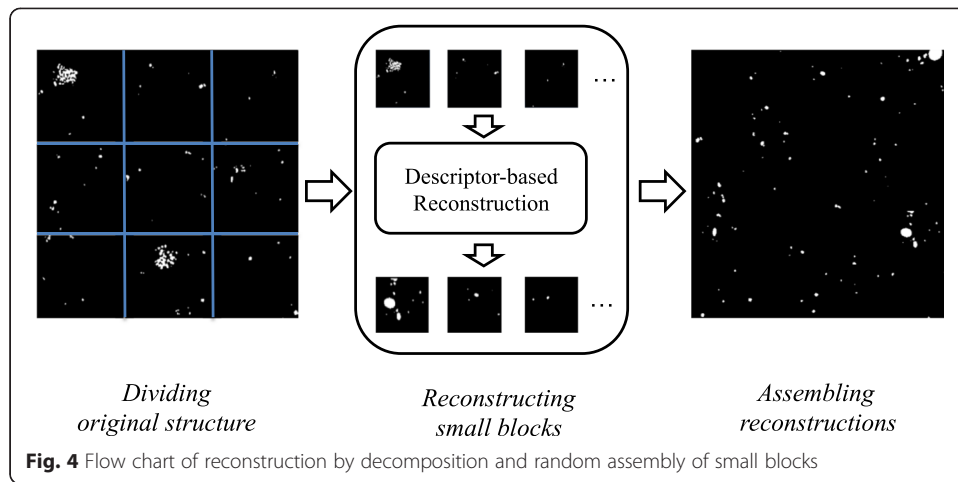
$$F = ax^2 + bxy + cy^2 + dx + ey + f. \quad (3)$$

Reconstruction using decomposition and reassembly

To deal with microstructures with local aggregates that are unevenly distributed over the whole image, we propose to first divide the image into subdomains and then reassemble small blocks of reconstructions to preserve local structural information. The proposed method follows three steps (shown in Fig. 4):

- 1) Divide the original microstructure into multiple equal size sub-blocks
- 2) Apply the 2D descriptor characterization and reconstruction algorithm to each sub-block
- 3) Randomly assemble the sub-block reconstructions to obtain the fully reconstructed microstructure

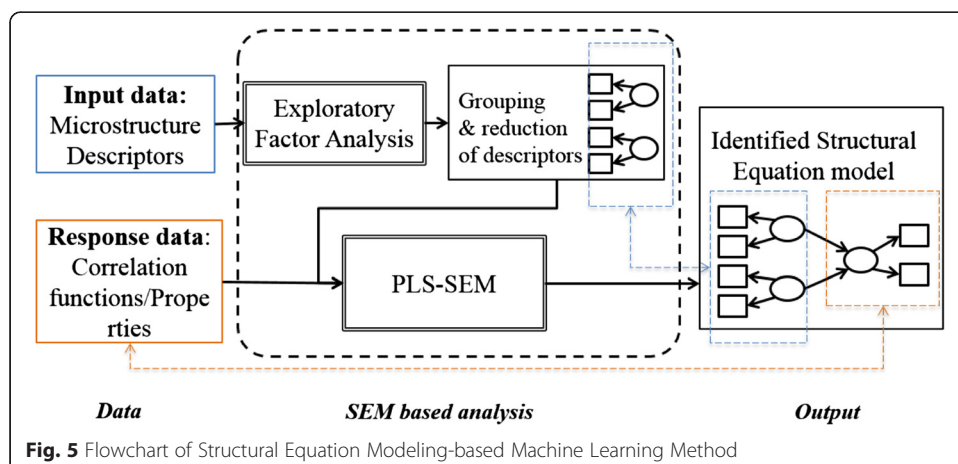
Our proposed method is inspired by the Morisita Index approach [27], which is used to analyze local versus global dispersions. The Morisita Index divides the original image using different sizes of small blocks, and then based on the number of particles in each



block, a weighted index is calculated to represent the dispersion status of an image. Here we need to choose an appropriate block size based on a specific problem, but the basic idea is similar: let the sub-blocks keep the local information, which would be lost if characterization and reconstruction were directly applied to the global region. The size of the sub-blocks may influence the reconstruction accuracy. In this study, it is found that when the block size is slightly larger than the largest clusters in the microstructure, satisfactory results can be obtained. A decomposition and reassembly strategy was also employed in the evaluation of structure-property relationships and proved to be effective [28]. One additional advantage of the proposed method is that in some sub-blocks, there may be no particles. The block is then maintained as pure matrix (void space) in the reconstruction to ease computation as well as to capture the void space feature which has been used in literature to quantitatively characterize material microstructure dispersion [29, 30] in low volume fraction systems.

Identification of key microstructure descriptors

The procedure of our proposed Structural Equation Modeling-based approach is shown in Fig. 5. Structural Equation Modeling is a multivariate data analysis method that is often used in social science for problems with latent layers and path structures [31].



Considering that microstructures are measurements of structural characteristics, the concept of a measurement model in Structural Equation Modeling can be applied. By introducing latent layers (structural features) in mapping input and output relations, we are able to identify the relationships and dependencies among different descriptors. The whole procedure contains two main parts: First exploratory factor analysis (EFA) [32] is used to reduce descriptors and group them where the latent factors are also identified. Second, with the identified structure, the Partial Least Squares (PLS) technique [33] is applied to estimate the coefficients in Structural Equation Modeling. PLS is shown to be advantageous for problems with a small number of samples and can predict responses accurately [34–36]. In the first step, the original descriptors are grouped under a few number of latent factors after using the EFA, and each latent factor relates to several descriptors (called indicators) that reflects the latent factor. The extracted latent factors can be considered as categories of microstructure features, described by descriptors, and the grouped structure reflects the correlation patterns of descriptors. In the second step, response data such as microstructure CF or material properties is added as the supervisory signal to identify the underlying descriptor-CF or descriptor-property relationship, solved using the PLS algorithm

Two steps are shown: EFA and PLS-SEM. Responses can include both CF and properties. In contrast to our proposed approach described above, the existing machine learning technique for identifying key microstructure descriptors pre-specifies the categories of microstructure features (e.g., *composition, dispersion, geometry*). Such classification is experience-based and can become arbitrary as key microstructural features may vary from one material system to another. In this work, exploratory factor analysis is used to classify the descriptors into several groups by identifying the common factors underlying the original data set. If the observed variables are X_1, X_2, \dots, X_n (microstructural descriptors such as minimum distance between fillers in the context of this work), the common factors are F_1, F_2, \dots, F_m (latent microstructural features, e.g., dispersion status), and the unique factors are U_1, U_2, \dots, U_n (the part of X that cannot be explained by F), the variables may be expressed as linear functions of the factors:

$$\begin{aligned} X_1 &= \lambda_{11}F_1 + \lambda_{12}F_2 + \dots + \lambda_{1m}F_m + U_1 \\ X_2 &= \lambda_{21}F_1 + \lambda_{22}F_2 + \dots + \lambda_{2m}F_m + U_2. \\ &\vdots \\ X_n &= \lambda_{n1}F_1 + \lambda_{n2}F_2 + \dots + \lambda_{nm}F_m + U_n, \end{aligned} \quad (4)$$

Each of these equations is a regression equation; factor analysis seeks to find the coefficients λ_{ij} (loadings on factors) that best reproduce the observed variables from the factors. If all coefficients are correlations and factors are uncorrelated, then the sum of the squared loadings for variable X_i , e.g., $\sum_j \lambda_{ij}^2$, shows the proportion of the variance of X_i explained by these factors. This is called the *communality*, and the larger the communality for each variable, the more successful the factor solution is.

The EFA helps us identify the common (latent) factors (F) that drive the variation of descriptors (X). Each latent factor can be associated with a specific microstructural feature. For example, *equivalent radius* and *pore size* are different measures of the clusters' sizes, where the cluster size can be considered a latent factor, and both equivalent

radius and pore size are observed indicators. The EFA process is implemented with three basic steps:

- Step 1: Determine the number of latent factors (exogenous variables) n
- Step 2: Conduct factor analysis with the n factors using proper rotation
- Step 3: Identify exogenous variables that are poor indicators of latent factors (uniqueness > 0.5) [32]

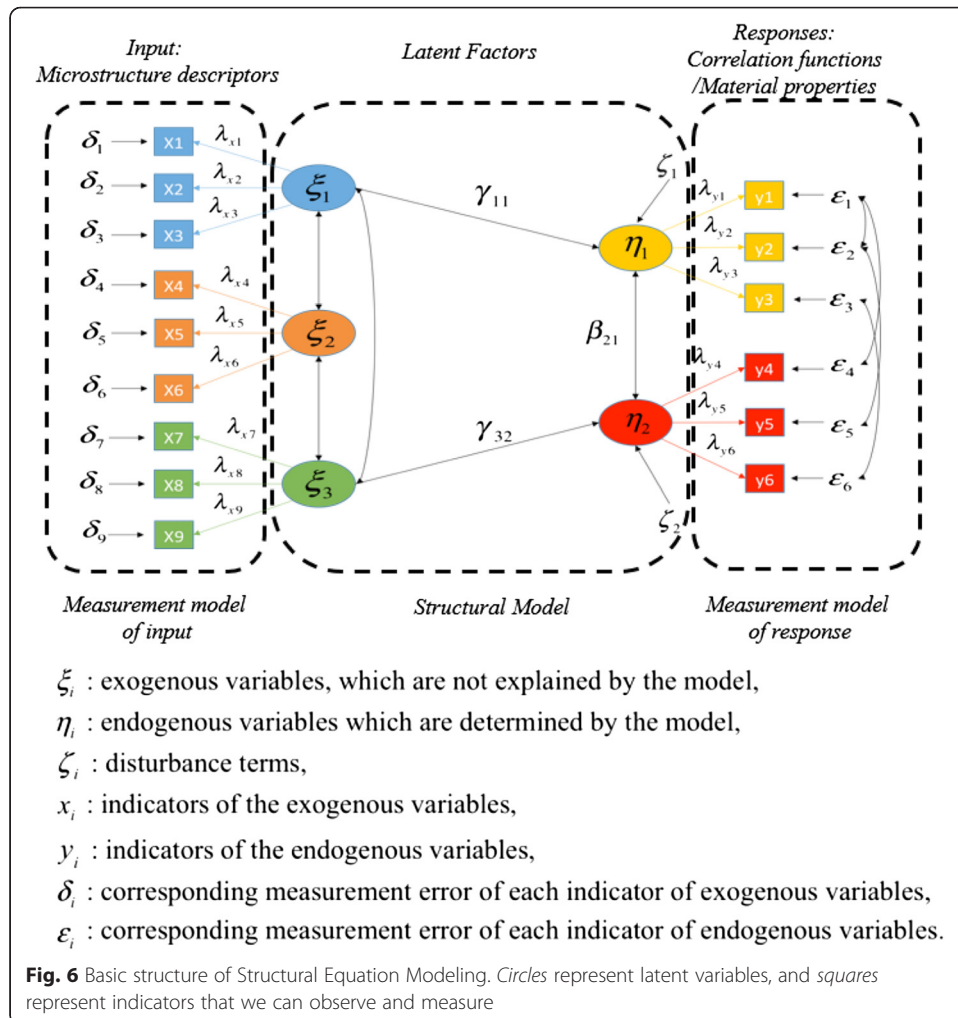
After identifying the proper structure model using EFA, a detailed Structural Equation Modeling analysis follows where the general structure can be found in Fig. 6. A detailed mathematical model of the presented structure is composed of three key equations:

$$\boldsymbol{\eta}_{(m \times 1)} = \mathbf{B}_{(m \times m)}\boldsymbol{\eta}_{(m \times 1)} + \boldsymbol{\Gamma}_{(m \times n)}\boldsymbol{\xi}_{(n \times 1)} + \boldsymbol{\zeta}_{(m \times 1)}, \tag{5}$$

$$\mathbf{y}_{(p \times 1)} = \boldsymbol{\Lambda}_{y(p \times m)}\boldsymbol{\eta}_{(m \times 1)} + \boldsymbol{\varepsilon}_{(p \times 1)}, \tag{6}$$

$$\mathbf{x}_{(q \times 1)} = \boldsymbol{\Lambda}_{x(q \times n)}\boldsymbol{\xi}_{(n \times 1)} + \boldsymbol{\delta}_{(q \times 1)}, \tag{7}$$

where m is the number of endogenous latent variables η , n is the number of exogenous



latent variables ξ , and p and q are the number of indicators (x and y) and for endogenous and exogenous variables, respectively. In our study, microstructure descriptors (inputs) are the indicators of exogenous latent variables and microstructure CFs and material properties (outputs) are the indicators of endogenous latent variables. Λ_y and Λ_x are the loading coefficient matrix for indicators y and x , ζ is a structural error vector, B is the relation matrix among endogenous variables η , and matrix Γ describes the relations between endogenous variable η and exogenous variable ξ . ε and δ are both measurement errors.

Equation (5) shows the mathematical relationship of the *structural model*, the relationship between latent variables, while Eqs. (6) and (7) both represent the *measurement model*, illustrating the relationship between latent variables and corresponding indicators.

In the context of material structure-property analysis, different categories of microstructure descriptors can be either pre-defined based on experience [12] or identified as the exogenous latent variables ξ_i for microstructure descriptors in the proposed Structural Equation Modeling structure after going through the EFA process. Latent variables are often not directly measured. For instance, *dispersion* can be a latent variable (exogenous variable ξ_i) but there is no explicit mathematical definition, while dispersion descriptors, such as nearest center distances and nearest boundary distances [7], can be viewed as indicators, represented by x 's. Different indicators (microstructure descriptors in this case) provide measurements of certain features of the microstructure. The error term, δ_i , in the general model can effectively take into account the errors introduced by the approximations in measurement. Considering measurement errors is another strength of the Structural Equation Modeling approach compared to other methods. Rather than assuming the different categories of descriptors are independent, the correlation between them can also be analyzed by studying the relationship among latent factors in the Structural Equation model.

Depending on the data available, endogenous latent variables η_i at the output side are related to material properties or statistical representations of microstructure (e.g., 2-point CF) in this study. If the microstructure 2-point CF is treated as an exogenous latent variable, then the indicators y_i can be the L_2 norm $\|S(r)\|_2$ of the 2-point CF [21] and the fitting parameters of the CF. The Debye exponential fitting function [37] shown in Eq. (8) is used in this work to represent the 2-point CF:

$$S(r) = \exp\left(-\frac{r}{a}\right) \quad (8)$$

where a is a fitting parameter that describes the shape of CF.

The structural error ζ_i describes unmodeled factors that may influence the endogenous variables η_i . If the exogenous variables ξ_i in the structured model cannot explain the endogenous variables η_i well, then a large structural error ζ may exist in the final model, which indicates that additional descriptors may need to be included.

Several different approaches are widely used to solve a structural equation. The first is covariance-based Structural Equation Modeling [38]. The other approach is the Partial Least Squares (PLS) algorithm [39], which is a soft modeling approach to Structural Equation Modeling with no restriction on the normality of data [23]. The PLS algorithm is especially effective for cases when a small number of samples are available [40]

and is used in our study. The PLS algorithm estimates the coefficients of both measurement and structural models by an iterative process. A brief diagram of the process is shown in Fig. 7 and the whole PLS algorithm is implemented using the software WarpPLS [41].

As a result of applying Structural Equation Modeling analysis, key microstructure descriptors are chosen as material design variables. Ideally, for each identified significant latent factor, we want to pick one descriptor as the best indicator (or microstructural design variable). The choice of multiple descriptors within one latent factor will lead to redundancy as multiple descriptors are often correlated.

Constructing structure-property relationship for microstructure design

With the identified set of descriptors, the Optimal Latin Hypercube Sampling (OLHS) [42] and the descriptor-based reconstruction algorithm can be used to generate a set of sample microstructures over the microstructure design space. Corresponding property data are obtained through finite element simulations and the descriptor-property model can be constructed using metamodeling techniques such as Kriging [43]. Figure 8

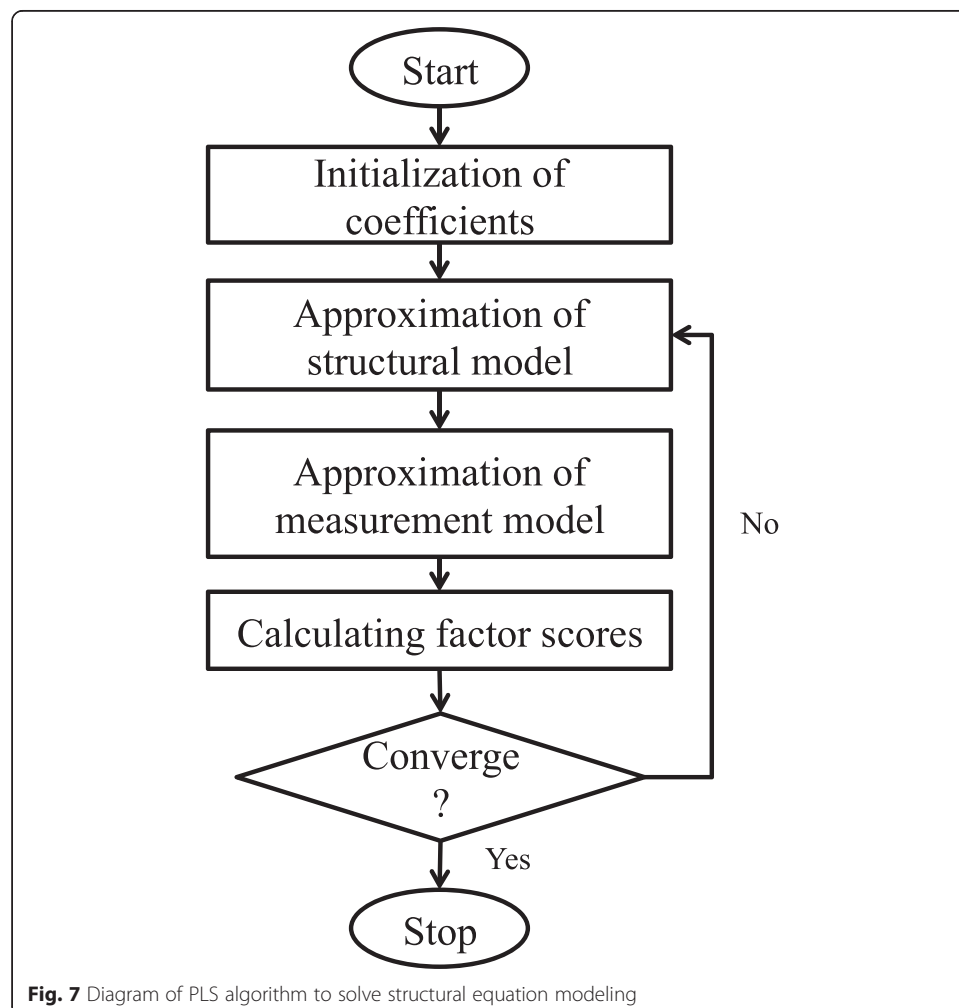
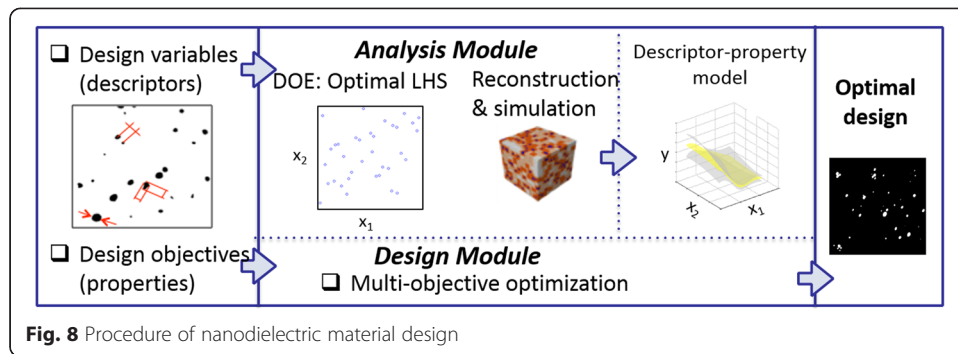


Fig. 7 Diagram of PLS algorithm to solve structural equation modeling



shows the general procedure to achieve optimal microstructure design using surrogate descriptor-property models. The procedure has been demonstrated in nanocomposite tire material design [12].

Nanodielectrics are widely used in energy storage applications, where the total energy depends on both permittivity and breakdown strength. For the simple case consisting of two parallel conductive plates separated by a dielectric with permittivity, ϵ , the total energy is determined from the following equation

$$E = \frac{1}{2} \epsilon A d U_d^2 \tag{9}$$

where ϵ is the dielectric constant, A and d are both geometric parameters of the capacitor, and U_d is the breakdown strength of the dielectric material. In order to improve the total energy storage, we need a high dielectric constant, ϵ , and high break down strength U_d . The breakdown of dielectric materials is a dynamic process, which makes it difficult to develop accurate simulation models.

In this study, we focus on the dielectric constant as the property of interest. For lossy materials, the dielectric constant is a complex value, which follows the form:

$$\epsilon = \epsilon' - j\epsilon'' \tag{10}$$

where the real part ϵ' represents the ability for energy storage and the imaginary part, ϵ'' , denotes the energy loss of the material. Loss angle, $\tan \delta$, is often used to represent the energy loss:

$$\tan \delta = \frac{\epsilon''}{\epsilon'} \tag{10a}$$

which describes the ratio of energy loss to energy storage.

As a simple illustration of microstructure design of nanodielectrics, the design objectives associated with the mechanical properties can be chosen as maximizing the real part ϵ' and minimizing the energy loss, $\tan \delta$. Previous work has shown that dielectric permittivity in polymer nanocomposites can be analyzed using a Prony Series approach adapted from viscoelasticity studies. This approach incorporates explicit consideration of microstructure dispersion as well as polymer interphase between the nanofillers and matrix into the Finite Element simulation [44]. Based on experimental results of bimodal brush grafted silica nanoparticles in an epoxy matrix, finite element modeling

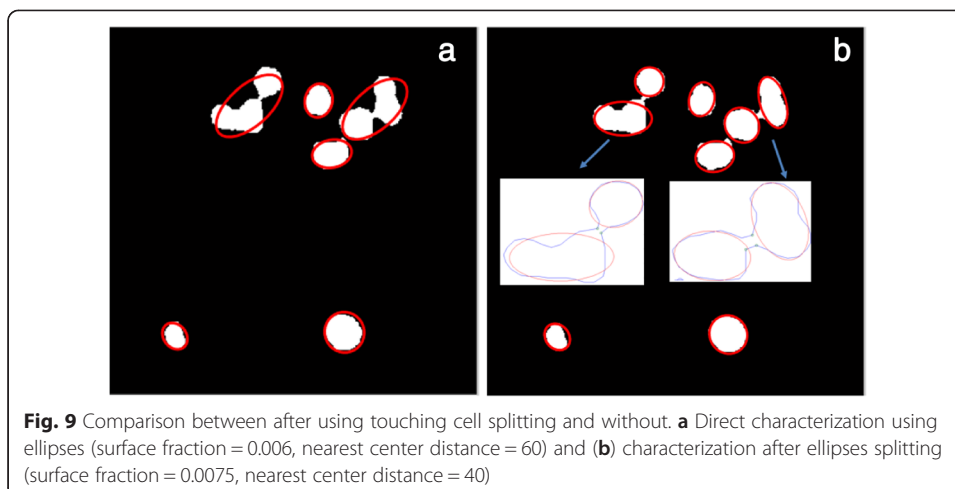
has been used to accurately capture the dielectric permittivity and loss angle measured in experiments by superposition of frequency-dependent dielectric relaxation constants. Optimization of nanodielectric materials can be achieved following the framework described in Fig. 8 once sufficient data are collected and multiple simulation property models are built.

Results and discussion

Characterization and reconstruction

Characterization results of a sample nanodielectric microstructure using the original descriptor-based approach without applying the splitting algorithm are presented in Fig. 9a, where we find that approximating the two irregularly shaped clusters by single ellipses introduces large errors. Figure 9b shows the result after using the proposed splitting algorithm. Clusters smaller than the primary particle size are considered to be a single ellipse. For this nanodielectric system, clusters with sizes larger than two primary particles (15 nm particle diameter) are considered as candidates for splitting.

As shown in Fig. 9b, the irregular clusters are each split into multiple ellipses, providing a better representation compared to the result in Fig. 9a where single ellipses are used to represent the irregular clusters. As a confirmation of improved accuracy using the splitting algorithm, we compare the interfacial area and the nearest center distance using the two methods. The interfacial area (2D boundary between the filler and matrix) in Fig. 9b is 0.0075 after using the splitting algorithm, which matches better with the real surface fraction 0.0078 of the original image, compared to 0.006 of the result in Fig. 9a without using the splitting algorithm. A similar observation is made for the characterized nearest center distance, which becomes 40 pixels after splitting versus 60 pixels before splitting. Nearest center distance reflects the local clustering behavior, and the “true” value is unknown as the evaluation depends on the way the cluster is characterized. The ellipse splitting algorithm implemented in this work is shown to be effective for splitting touching clusters and offering more accurate characterization. This splitting algorithm is utilized for all microstructure characterizations in the following sections of this paper.



After applying the splitting algorithm, the following descriptors are used to characterize the nanodielectric system for the subsequent reconstructions:

- Volume fraction (deterministic)
- Nearest center distance (mean and variance)
- Aspect ratio (mean, variance, normal distribution)
- Cluster area (mean, exponential)

Figure 10 shows two image samples chosen from the nanodielectric for reconstruction. The microstructure in sample 1 has a few small local clusters and also some large particle-free spaces with volume fraction at a level as low as 0.53 %. Sample 2 has some large aggregates, which is a very common feature over the samples collected. The physical size of the image is about $1 \times 1 \mu$ and the pixel size is 2000×2000 .

The statistical information characterized from the two original microstructures is summarized in Table 1. It is observed that the nearest center distance (both mean and variance) of sample 2 is much smaller than that of sample 1 ($79 < 124$), which reflects the local aggregation behavior in sample 2. Since sample 1 does not exhibit strong local aggregations, six reconstructions are generated (see Fig. 11) using the original descriptor-based approach with the split algorithm but without applying the proposed decomposition and reassembly strategy. For ease of comparison, the resolution of reconstruction is set to be exactly the same as the original, 2000×2000 pixels. While larger reconstruction windows always result in more accurate statistics than smaller ones, keep in mind that when the size of reconstruction increases, the computational time increases dramatically, especially for 3D reconstructions. Comparing the reconstructions of sample 1 with the original microstructure, we observe many similarities. First, the distributions of cluster sizes are identical; there are a small number of big clusters and the majority are small clusters. Second, the local clusters are captured in the reconstructions while some large particle-free spaces are observed.

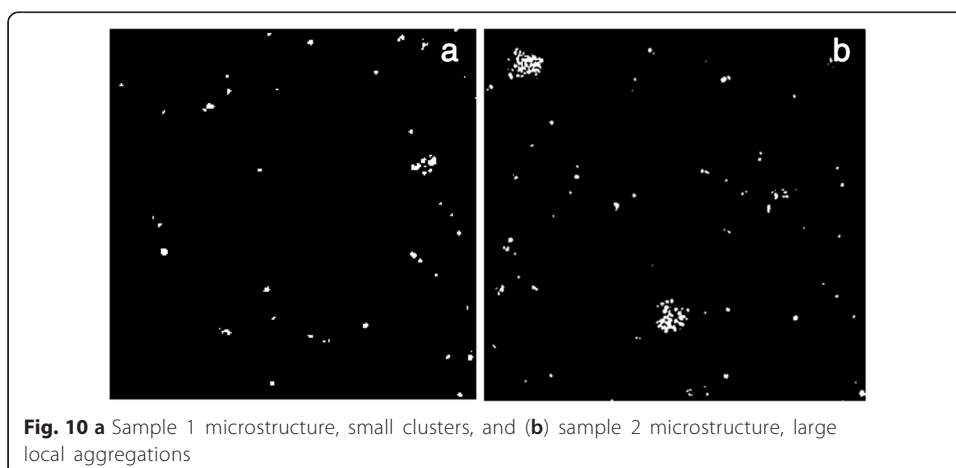


Table 1 Descriptor information of the two sample microstructures (unit of length: nm)

	Sample 1	Sample 2
Volume fraction	0.53 %	0.9 %
Nearest center distance	1st mean = 124, 1st var = 15,410	1st mean = 79, 1st var = 4151
Aspect ratio	Mean = 0.7513, var = 0.0234	Mean = 0.9701, var = 0.0315
Cluster area	Mean = 200	Mean = 10,120

To evaluate the accuracy of reconstructions, the 2-point CF from reconstructions are compared to the one from the original image. The relative error in L_2 norm is used to measure the deviation:

$$\text{err} = \frac{\|S_2'(r) - S_2(r)\|_2}{\|S_2(r)\|_2} \tag{11}$$

where $S_2(r)$ is the target 2-point CF and $S_2'(r)$ is the 2-point CF of reconstruction. The average error from six reconstructions is found to be 5 %, which is acceptable for this low volume fraction material system.

For sample 2, with large local clusters, the proposed decomposition and reassembly strategy using small blocks are implemented and compared using the original descriptor-based approach with the split algorithm for the whole image. It is noted that without applying the proposed decomposition and reassembly strategy, the two big clusters shown in Fig. 10b are not captured by the reconstructed microstructure. Clusters in the reconstruction shown in Fig. 12a are much more evenly dispersed than the target image, even though a few big clusters do appear in reconstruction. The difference between the 2-point CF is large and the relative error calculated with Eq. (11) is over 40 %. The result is not surprising because when the aggregates are not statistically representative over the window size, e.g., an image with a very small number of large aggregates, the reconstruction cannot reproduce the results. Figure 12b shows one reconstruction sample from using the proposed decomposition and reassembly algorithm with 64 sub-blocks. Two large clusters and more particle-free spaces are observed in the reconstruction, which is closer to the original microstructure compared to Fig. 12a.

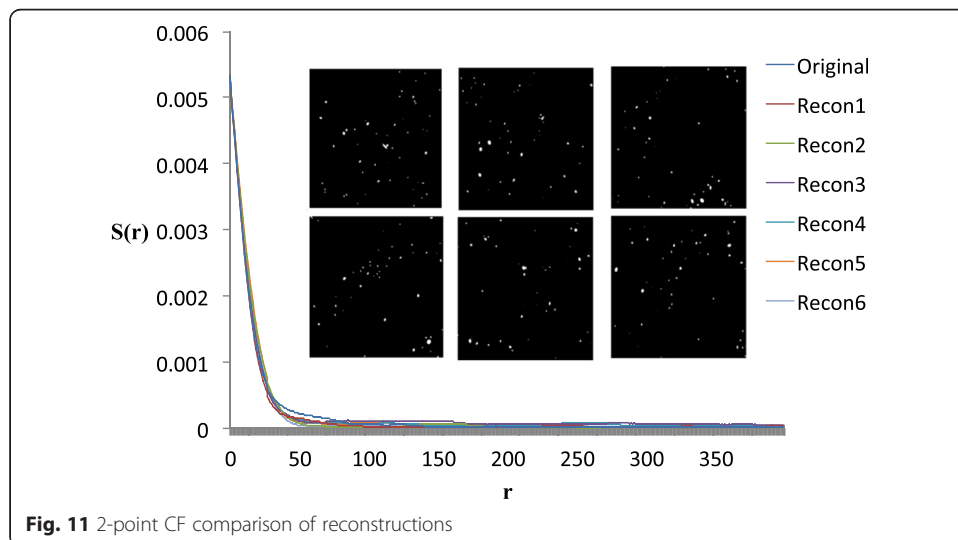
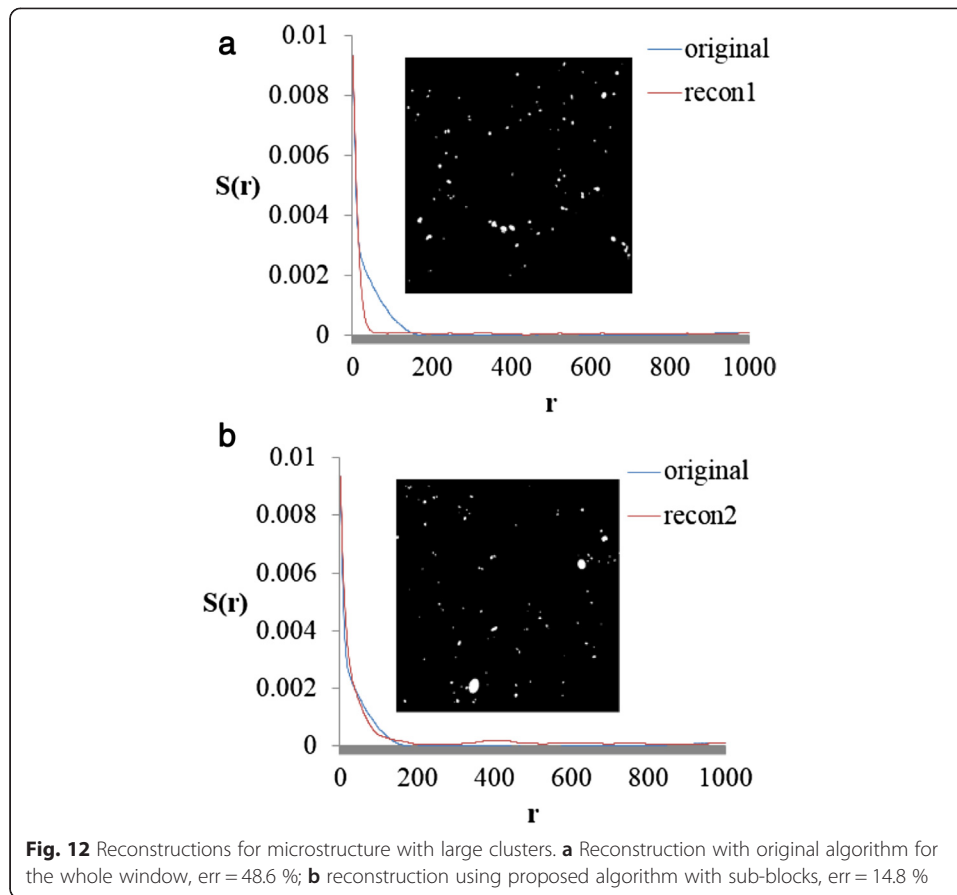


Fig. 11 2-point CF comparison of reconstructions



By comparing Fig. 12a, b, it is noted that the 2-point CF obtained using our proposed decomposition and reassembly strategy matches much more closely than using the original algorithm, especially in the short range from $r = 50$ to 100. The relative error achieved is 14.8 %, which is a big improvement compared to 48.6 % using the original approach. The results show that the uneven local information is maintained through the proposed strategy of using small blocks. It should be noted that when assembling the small blocks, a totally random sequence is applied in our study. Omitting the relationship between the sub-blocks is acceptable here for two reasons: (1) The large clusters are sparse in the microstructure images; therefore, it is difficult to come up with a statistical characterization that is representative for the whole image. (2) For such a low volume fraction system, it has been observed that the main differences among 2-point CF occur in the short distance range, which has been captured by the information obtained from individual small blocks. 2-point CF are usually oscillating with several peaks and valleys. The location of the first deepest drop corresponds to the size of local clusters and the peaks at longer distance relate to certain global periodical patterns. As for this case study, no obvious long distance pattern can be observed, so it is not necessary to consider the higher order block-block relationships. In real implementation, the best results will be achieved by randomly assembling the small blocks multiple times and choosing the best match for the target CF, to compensate for the lack of block-block characterization.

Identification of key descriptors from images using the Structural Equation Modeling approach

In this paper, we illustrate the use of the Structural Equation Modeling approach based on the information gathered from microstructure images only, where the CF are used as supervisory responses, and the L_2 norm $\|S(r)\|_2$ of the 2-point CF and the fitting parameters described in Eq. (8) are used as indicators. Image-driven analysis allows us to keep the generality of the results (key descriptors), independent from the properties of interest. If Structural Equation Modeling analysis is applied by using the property as responses, different material properties may result in different key structural features. Since structure-property simulations are expensive, image-based Structural Equation Modeling analysis for identifying key structure descriptors is recommended. To start with, the full set of descriptors considered for particle-based microstructural systems are first gathered from the literature related to hard or soft materials. They are classified and marked under three categories: (1) *composition*, (2) *dispersion*, and (3) *geometry* [21], in Table 2. The majority of the 29 descriptors are statistical, for which two moments are used to represent the entire distributions. As training samples, 117 TEM images of low volume fraction nanodielectric materials (0.5 % to 3 %) were collected.

The exploratory factor analysis (EFA) approach presented in the “Methods” section and the associated three steps are first followed to identify the proper number of latent factors and group the microstructure descriptors (indicators) based on their associations with the latent factors. When applying the EFA approach, only the data collected on microstructure descriptors from 117 images is used. Methods for choosing the number of latent factors have been well studied and three widely used criteria, *K1 method*

Table 2 Descriptor set for statistical learning. Reference are provided for those descriptors without explicit meaning

Descriptor	Definition	Type
Composition		
VF	Volume fraction	Deterministic
Dispersion		
ncd	Cluster's nearest surface distance	Statistical
nbd	Cluster's nearest center distance	Statistical
ornang	Principle axis orientation angle [51]	Statistical
intph	Surface area of matrix phase	Deterministic
N	Cluster number	Deterministic
Loc_VF	Local VF of Voronoi cells [52]	Statistical
Geometry		
pores	Pore sizes (inscribed circle's radius) [53]	Statistical
area	Cluster area	Statistical
rc	Equivalent radius, $rc = \sqrt{A/\pi}$	Statistical
comp	Compactness [54]	Statistical
rnds	Roundness [55]	Statistical
eccen	Eccentricity [55]	Statistical
els	Aspect ratio [56, 57]	Statistical
rectan	Rectangularity [55]	Statistical
tsst	Tortuosity [55]	Statistical

(eigenvalue) [45], *Non-graphical Cattell's Scree Test* (optimal coordinates and acceleration factor) [46], and *Horn's Parallel Analysis* [47], are employed in Step 1 of EFA to build confidence in the result.

Based on the results shown in Fig. 13, the number of microstructure latent factors is determined to be 5 for our case study. Because the major purpose of the EFA is to group descriptors, the cross loadings of descriptors on latent factors should be minimized. Hence in Step 2 of EFA, the oblique Promax rotation method [48] is chosen to adjust orthogonal factors so that the small loadings can be made closer to 0. With the Promax rotation, we maximize the number of input variables (descriptors) that have only one high loading on a specific latent factor. The EFA results are shown in Table 3. The five latent factors (meanings explained in next paragraph) explain over 80 % of the variances of the original descriptor set. The loadings of input descriptor variables on latent factors can be found in the first five columns, and the largest loading in each row is in italics. The last two columns show the *uniqueness* of input variables and the *complexity* respectively. Uniqueness is measured by U_i^2 in Eq. (4), and small value of uniqueness means factors explain input variables well. In the table, if we take a look at the row of *ornang1*, all the loadings are very small and the uniqueness is 0.96, which is very close to 1. Thus we can conclude that the variation of *ornang1* is not well explained by these latent factors in our model. *Complexity* [49] measures the number of relevant factors for each input variable. Higher complexity means the variable is relevant to multiple factors and cannot be represented by a single factor.

In Step 3 of the EFA procedure, based on the rule that at least half of the variance of an independent variable should be explained by a latent factor (uniqueness ≤ 0.5), we can identify poor factor indicators (underlined) and withdraw them from our data set. Going through steps 1 to 3 in EFA, we reduced the number of characterization parameters from 29 to 19 and associate them to five latent factors. Examining the results, we can relate each factor to a physical interpretation: Factor 1 represents the *size of clusters*, with 6 descriptors as indicators: cluster area (*area1*, *area2*), pore size (*pores1*, *pores2*), and equivalent radius (*rc1*, *rc2*). Factor 2 represents the *distribution status*,

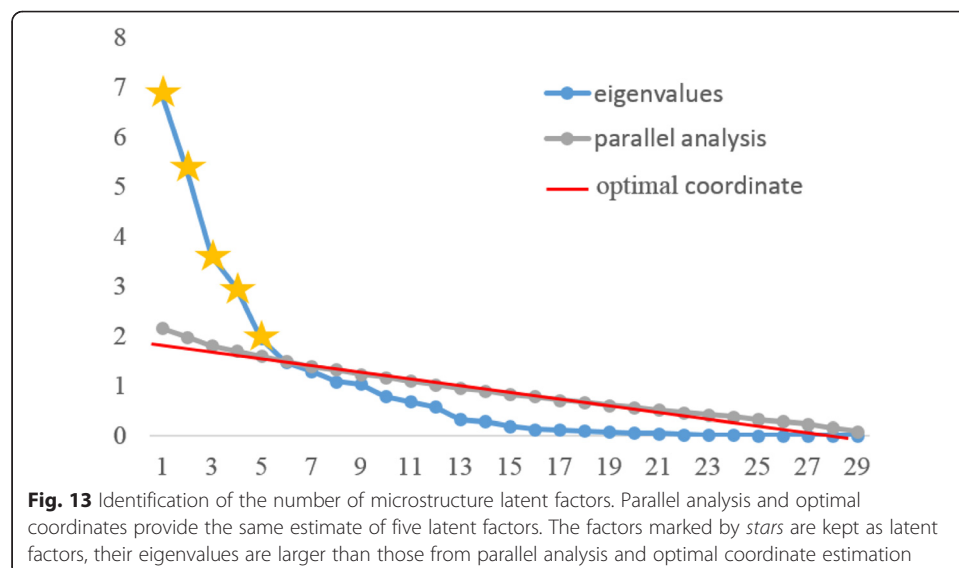


Table 3 Results of EFA (loading, uniqueness, and complexity). The meaning of descriptors can be found in Table 2. Indices 1 and 2 indicate the mean and variance of the corresponding descriptor, respectively, e.g., *area1* stands for the mean of clusters area

	F1, cluster size	F2, distribution	F3, composition	F4, geometry1	F5, geometry2	Uniqueness**	Complexity
<i>area1</i> *	<i>0.99</i>	-0.03	-0.08	-0.04	-0.09	0.0066	1
<i>area2</i>	<i>0.87</i>	-0.02	0.19	-0.03	0.25	0.2016	1.3
<i>comp1</i>	<i>0.05</i>	-0.06	0.13	-0.01	<i>0.92</i>	0.1244	1.1
<i>comp2</i>	0.06	0.15	0.13	0.23	-0.28	<i>0.7996</i>	3.2
<i>eccen1</i>	0.08	-0.03	0.08	0.19	-0.43	<i>0.7363</i>	1.6
<i>eccen2</i>	0.09	0.24	0.12	-0.12	0.15	<i>0.9222</i>	3.3
<i>els1</i>	0.27	-0.01	0.13	0.24	-0.32	<i>0.6794</i>	3.2
<i>els2</i>	0.12	0.23	0.06	0.39	0.15	<i>0.7368</i>	2.3
<i>locvf1</i>	0.37	-0.02	<i>0.57</i>	-0.1	-0.22	0.397	2.1
<i>locvf2</i>	0.36	0.09	0.23	0.02	-0.14	<i>0.7351</i>	2.2
<i>nbd1</i>	0.11	<i>0.69</i>	-0.38	-0.01	0.23	0.0913	1.9
<i>nbd2</i>	-0.17	<i>1.02</i>	0.08	-0.03	-0.17	0.0544	1.1
<i>ncd1</i>	0.25	<i>0.65</i>	-0.38	-0.01	0.16	0.0949	2.1
<i>ncd2</i>	-0.13	<i>1.01</i>	0.08	-0.04	-0.18	0.0496	1.1
<i>ornang1</i>	-0.04	-0.09	-0.03	0.16	0.04	<i>0.9673</i>	2
<i>ornang2</i>	-0.03	-0.02	0.07	0.15	0.28	<i>0.8921</i>	1.7
<i>pores1</i>	<i>0.92</i>	-0.09	-0.35	-0.1	-0.02	0.2054	1.3
<i>pores2</i>	<i>0.92</i>	0.01	-0.04	0	0.06	0.1733	1
<i>rc1</i>	<i>0.88</i>	-0.01	-0.22	-0.06	-0.28	0.0704	1.4
<i>rc2</i>	<i>0.97</i>	-0.02	0.05	-0.01	0.11	0.0905	1
<i>rctan1</i>	-0.1	-0.03	-0.09	<i>1</i>	-0.04	0.0075	1
<i>rctan2</i>	-0.1	-0.05	-0.1	<i>1</i>	-0.04	0.015	1
<i>rnds1</i>	0.03	-0.06	-0.02	-0.1	<i>0.75</i>	0.4154	1.1
<i>rnds2</i>	0.21	0.01	0.06	0.21	0.25	<i>0.8562</i>	3.1
<i>ttst1</i>	0.05	-0.08	0.15	0.51	0.44	<i>0.5319</i>	2.2
<i>ttst2</i>	0.02	0.03	-0.09	<i>0.85</i>	-0.21	0.1797	1.2
<i>intph0</i>	-0.07	-0.02	<i>0.94</i>	-0.09	0.01	0.0992	1
<i>n</i>	-0.37	0.03	<i>0.91</i>	-0.08	0.21	0.0726	1.5
<i>vf</i>	0.49	-0.03	<i>0.74</i>	-0.08	0.15	0.0977	1.8

*Highest descriptor loading in each row is made italic, and it indicates strong association between the descriptor and the latent factor

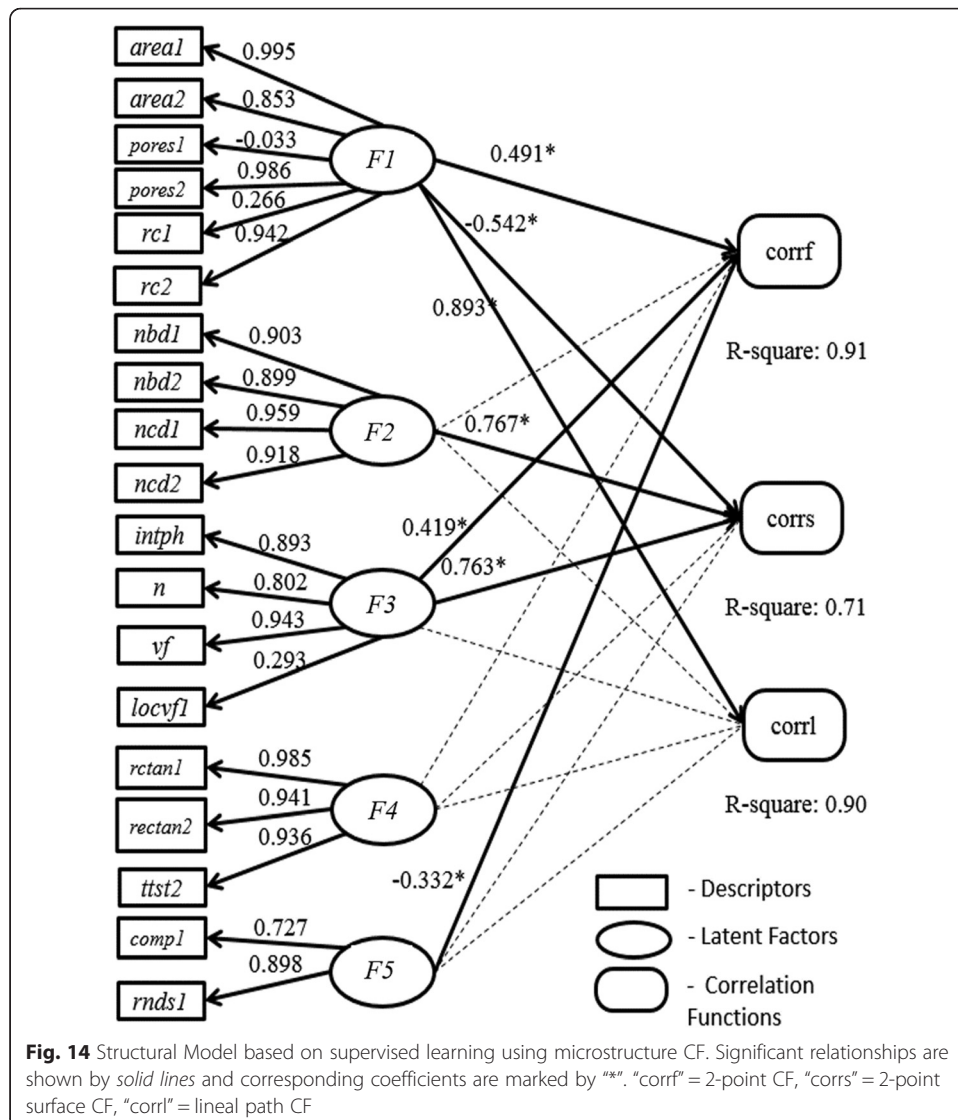
**Uniquenesses larger than 0.5 are made italic and the corresponding descriptors are not considered in later analysis. Large uniqueness means low association between descriptor and latent factor

with the nearest neighbor distance such as nearest boundary distance (*nbd*) and nearest center distance (*ncd*) as the indicator. Factor 3 describes the composition information, including volume fraction (*vf*), interfacial fraction (*intph*), number of clusters (*n*), and local volume fraction (*locvf1*). Volume fraction clearly describes the *composition*, and the other three describe higher order composition information. Factors 4 and 5 represent two *geometric characteristics*: Factor 4 is associated with rectangularity (*rctan1*, *rctan2*), and tortuosity (*ttst2*); Factor 5 is associated with compactness (*comp1*) and roundness (*rnds1*).

With the identified associations between microstructure descriptors and latent factors, and the three parameterized CF (2-point, 2-point surface, and linear path) as responses for supervised learning, a PLS algorithm is applied to identify the structural

equation model, and the final results are visualized in Fig. 14. It is observed that Factor 4 has no significant influence on all three CFs. Factor 5 only has a weak impact (-0.332) on the 2-point CF, but not on the other two CFs. The above indicates that the cluster geometry information is not critical for the microstructures of the nanodielectric system in this study. Factors 1 (size of clusters) and 3 (composition) have significant influence on CFs (large coefficients such as 0.893, 0.763 and P value <0.001). Influence from Factor 2 (distribution status) mainly goes toward the surface CF (corr_s), with 0.767 as the coefficient. In addition, the R-squared for all three responses are very high (average over 0.8), indicating the latent factors in this model explain well the variation of responses (CF).

The obtained Structural Equation Model is verified based on the physical meaning of factor coefficients. For example, Factor 1 represents the size of clusters and it is meaningful that it has a negative effect (-0.542) on the surface correlation and a strong positive effect (0.893) on the lineal path correlation. Intuitively, a larger cluster size leads to smaller surface area and larger lineal path. Based on the



Structural Equation Model analysis, a potential set of material design variables are chosen by including four descriptor variables, each underlines Factor 1, Factor 2, Factor 3, and Factor 5, respectively. Based on the loadings of each descriptor with respect to each latent factor, the most significant set is identified to be *area1* (0.995, average cluster area) for Factor 1, *ncd1* (0.959, average nearest center distance) for Factor 2, *vf* (0.943, volume fraction) for Factor 3, and *rnds1* (0.898, average cluster roundness) for Factor 5.

The Structural Equation Model approach provides a clear association of descriptors and factors that are identified to minimize dependency through factor analysis. In contrast, if we use the existing supervised ranking method based on the Relief algorithm [21], we will run into several issues. The first problem is there is no subjective criterion to determine how many descriptors to keep only with the ranking information. Second, the redundancy issue among the top ranked descriptors cannot be properly addressed. Specifically, the top four (4) ranked descriptors from the Relief ranking algorithm based on the contribution of individual descriptors to responses for the same test case is identified to be *vf*, *area1*, *pores2*, and *rc2*. A follow-up check of the correlations among these three descriptors as shown in Table 4 indicates strong correlations with the average above 0.9. From the Structural Equation Model analysis shown in Fig. 14, *area1*, *rc2*, and *pores2* belong to the same latent category (Factor 1) and their loading factors (0.995, 0.942, 0.986) are very close to each other; therefore, choosing all three of them as key descriptors becomes redundant. Even though correlations among descriptors can be identified first before applying the Relief algorithm, selecting what descriptors to keep for data mining is still a problem [21]. Moreover, with the Relief ranking algorithm, it is very likely that we withdraw important descriptors that have more significant influence on the latent factors but are ranked relatively low in the whole list of descriptors. The Structural Equation Model-based method does not have these issues because highly correlated descriptors are reduced to a single latent factor in the EFA step and the importance of each descriptor can be reflected by factor loadings, based on which the key descriptors can be selected for each latent factor. The proposed method hence provides much more insight into the data as well as helps to understand and interpret complex relationships.

Table 4 Correlation comparison of chosen descriptors. Proposed and prior ranking algorithm, high correlation among *area1* (average cluster area), *pores2* (variance of pore size), and *rc2* (variance of equivalent radius)

Structural Equation Modeling-based analysis	<i>vf</i>	<i>area1</i>	<i>ncd1</i>	<i>rnds1</i>
<i>Vf</i> —volume fraction				
<i>area1</i> —average cluster area	0.46			
<i>ncd1</i> —average nearest center distance	−0.32	0.33		
<i>rnds1</i> —average cluster roundness	0.08	−0.23	−0.10	
Prior ranking algorithm [21]	<i>vf</i>	<i>area1</i>	<i>pores2</i>	<i>rc2</i>
<i>Vf</i> —volume fraction				
<i>area1</i> —average cluster area	0.56			
<i>pores2</i> —variance of pore size	0.43	0.90		
<i>rc2</i> —variance of equivalent radius	0.54	0.93	0.91	

Validation using reconstruction and property simulations

To further validate that the four identified key descriptors retain the majority of the structural information, quantitative comparisons were made between the original 2D microstructure and reconstructions using identified key descriptors, through comparing CFs and simulating the dielectric properties for the epoxy-silica system [4]. Eight representative microstructures are chosen for this validation, and three reconstructions are generated for each of the eight microstructures to account for reconstruction uncertainty. The comparison of CFs are shown in Fig. 15 for two examples, where the four identified key descriptors from the Structural Equation Modeling approach are used to reconstruct 2D microstructures. It is observed that the CFs of reconstructions match well with those of original microstructure. The property simulation results are shown in Table 5, and the differences between reconstructions and the original images are measured by a relative error in terms of the two interested dielectric properties. With an average error at level 0.44 %, the identified descriptors are proven to be capable of capturing the key structural features that affect the dielectric constant ϵ' . The average error of loss angle $\tan \delta$ is 3.5 %, which is acceptable considering reconstruction uncertainty and simulation errors.

We also compare the capabilities of predicting material properties using these two different microstructural representations (the correlation function (CF)-based approach and the key descriptor-based approach). A linear regression model is chosen for simplicity and the analysis is based on collected nanodielectric images and simulated properties. Model fitting results are presented in Table 6. It is observed that both models have high prediction accuracy and the model using CF shows slightly better performance in predicting both dielectric constant and loss angle, which is reasonable since the key descriptors are identified based on CF. In conclusion, the identified four key descriptors capture the structural information and provide satisfactory property prediction accuracy.

The effects on material properties of each descriptor can be estimated from the standardized coefficients in the fitted linear regression model (shown in Table 5). It is

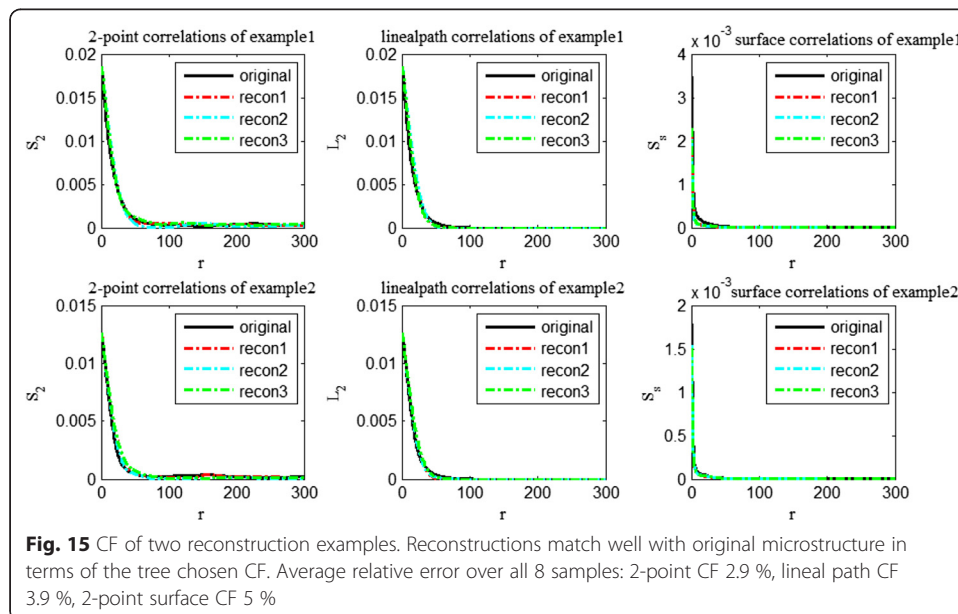


Table 5 Comparison of dielectric properties of the original and reconstructed images. Eight samples are chosen; properties are averaged over five reconstructions for each sample

	Dielectric constant ϵ'			Loss angle $\tan \delta$		
	Original	Reconstruction (average)	Error (%)	Original	Reconstruction (average)	Error (%)
1	4.215	4.204	0.254	0.0167	0.0161	3.50
2	4.084	4.084	0.016	0.0173	0.0164	4.74
3	3.926	3.941	0.384	0.0190	0.0185	2.78
4	3.897	3.903	0.168	0.0192	0.0190	0.92
5	4.109	4.173	1.546	0.0167	0.0158	5.36
6	3.910	3.920	0.253	0.0191	0.0188	1.59
7	3.962	3.971	0.212	0.0185	0.0181	2.14
8	3.981	4.009	0.709	0.0181	0.0175	3.24
Average			0.443	Average		3.50

interesting that even through the image-based supervised learning based on the Structural Equation Modeling approach identifies the average nearest center distance, $ncd1$, as one of the four key descriptors, the influence of $ncd1$ is not significant for both properties in this case study. This can be explained by the fact that in the studied nano-dielectric system, clusters are sparsely distributed, where the interactions between clusters are very weak. In that case, the variation of the nearest distance will not strongly affect material properties. The influence of average roundness, $rnds1$, on the two properties of interest is much smaller compared with that of average clusters area, $area1$, and volume fraction, vf . Smaller cluster area and larger volume fraction lead to better dielectric performance: higher energy storage capability (high ϵ') and smaller dielectric loss (small $\tan \delta$), which is visualized in Fig. 16. This observation is consistent with the findings in the literature that systems with small particles have high surface area-to-volume ratio, which is critical in determining the properties of nano-filled materials [50]. In general cases, the structure-property (s-p) relationship can be more complicated so that we may need to fit nonlinear models, such as Kriging meta-models. Our ongoing work is focused on establishing processing-structure (p-s) relationship. Once the whole processing-structure relationship is completed, we can link the p-s and s-p relationships together to achieve optimal design of the material.

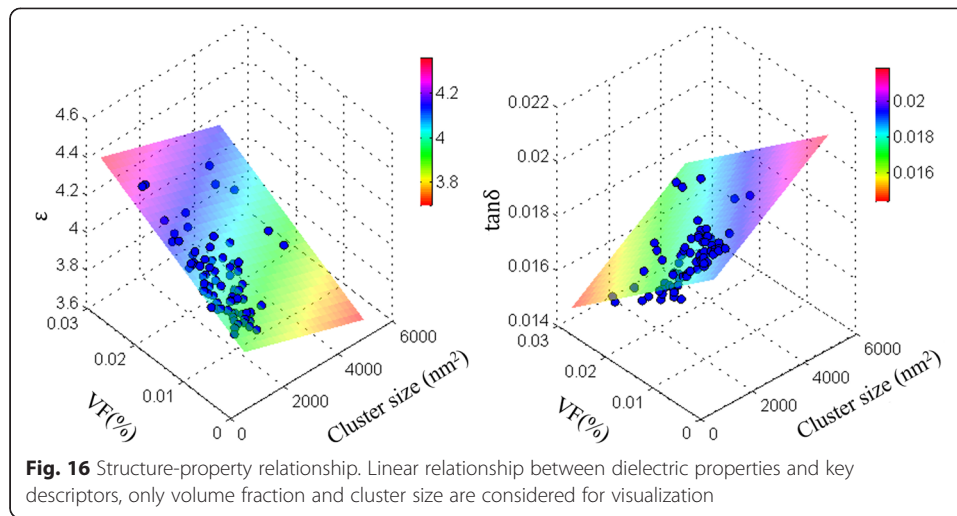
Conclusions

In this paper, new characterization, reconstruction, and key microstructure feature identification techniques are developed to support the computational design of nanodielectric systems. For design representation, a descriptor-based characterization and

Table 6 Results of linear model fitting

Model	CF (six parameters)		Key descriptors (four)		Standardized coefficients of descriptors			
	Prediction error	R-squared	Prediction error	R-squared	Average cluster area	Volume fraction	Average nearest distance	Average roundness
ϵ'	5.53e-04	0.95	8.36e-04	0.93	-0.419 ^a	1.060 ^a	0.0008	0.096 ^a
$\tan \delta$	1.12e-07	0.91	7.5e-08	0.88	0.614 ^a	-1.034 ^a	0.0043	-0.048

Prediction errors are estimated by 10-fold cross validation; model for CF contain six variables; standardized coefficients of the model using key descriptors are provided and significant ones are marked by ^a, at confidence level 0.95



reconstruction method is employed and tailored for a low volume fraction nanodielectric system with uneven local aggregations and irregularly shaped clusters. To handle special microstructures with large local aggregates, we propose a new decomposition and reassembly strategy, based on which the reconstruction accuracy is greatly improved. We also incorporate a touching cell splitting algorithm into the descriptor-based method to deal with irregularly shaped clusters to achieve more realistic characterization. To simplify the material design process and minimize the redundancy among design variables, a new Structural Equation Model-based method is developed to identify key descriptors. To keep the results independent from the material properties of interest, the analysis presented in this paper is based on information from the microstructure images (CF). According to the fitted Structural Equation Model, in which descriptors are classified into five groups based on the identified latent factors, we find *volume fraction*, *cluster size*, *nearest center distance*, and *cluster roundness* to be a sufficient set of descriptors to represent the structural features of the very low volume fraction nanodielectric system in this research. The relationship between the microstructure and properties are explored based on the epoxy-silica system and a close to linear relationship is observed between dielectric permittivity and the identified key descriptors.

In a future work, more image data of nanodielectric material systems with a wider range of volume fraction will be collected and simulation models for predicting all important dielectric properties will be included. In addition, the design problem will be extended to include both permittivity and breakdown strength as objectives. To make the tradeoff between the two, the Pareto frontier will be used to first identify a set of non-dominated (best achievable) optimal solutions. In addition, the Structural Equation Model-based method can also be applied to find the relations between descriptors and certain properties, which can then be directly used as predictive models in material design. Processing conditions will be taken into consideration to establish the mapping relations across the chain of processing-structure-property to ensure the manufacturability of new nanodielectric materials.

Availability of supporting data

Data presented in this work will be made available upon request.

Competing interests

The authors declare that they have no competing interests.

Authors' contributions

Y. Z performed the microstructure characterization and reconstruction, and proposed the structural equation modeling based approach for identifying key descriptors. H. Z developed the finite element model for simulating dielectric property. I. H made material samples and provided experimental data. L. B, L. S and W. C supervised the project. All authors read and approved the manuscript.

Acknowledgements

The support from NSF for this collaborative research: CMMI-1334929 (Northwestern University) and CMMI-1333977 (RPI), is greatly appreciated.

Author details

¹Northwestern University, Evanston, USA. ²Rensselaer Polytechnic Institute, Troy, USA.

Received: 18 December 2014 Accepted: 20 November 2015

Published online: 22 December 2015

References

1. Nalwa HS (1999) Handbook of low and high dielectric constant materials and their applications, two-volume set, Academic Press, Waltham, Massachusetts, USA
2. Barber P, Balasubramanian S, Anguchamy Y, Gong S, Wibowo A, Gao H, Zur Loye HC (2009) Polymer composite and nanocomposite dielectric materials for pulse power energy storage. *Materials* 2(4), 1697–1733
3. McPherson JW, Kim J, Shanware A, Mogul H, Rodriguez J (2003) Trends in the ultimate breakdown strength of high dielectric-constant materials. *Electron Devices, IEEE Transactions on*, 50(8):1771–1778
4. Ding HZ, Varlow BR (2004) Effect of nano-fillers on electrical treeing in epoxy resin subjected to AC voltage. In: *Electrical Insulation and Dielectric Phenomena, 2004. CEIDP'04. 2004 Annual Report Conference on. IEEE*, pp 332–335
5. Olson GB (1997) Computational design of hierarchically structured materials. *Science* 277(5330):1237–1242
6. McDowell DL, Olson GB (2009) Concurrent design of hierarchical materials and structures. In: *Scientific Modeling and Simulations*, Springer Netherlands, pp 207–240
7. Xu H, Dikin DA, Burkhart C, Chen W (2014) Descriptor-based methodology for statistical characterization and 3D reconstruction of microstructural materials. *Comput Mat Sci* 85:206–216
8. Torquato S, Stell G (1982) Microstructure of two-phase random media. I. The n-point probability functions. *J Chem Phys* 77(4):2071–2077
9. Torquato S, Stell G (1983) Microstructure of two-phase random media. II. The Mayer–Montroll and Kirkwood–Salsburg hierarchies. *J Chem Phys* 78(6):3262–3272
10. Lu B, Torquato S (1992) Lineal-path function for random heterogeneous materials. *Phys Rev A* 45(2):922
11. Torquato S, Beasley J, Chiew Y (1988) Two-point cluster function for continuum percolation. *J Chem Phys* 88(10):6540–6547
12. Xu H, Li Y, Brinson C, Chen W (2014) A descriptor-based design methodology for developing heterogeneous microstructural materials system. *J Mech Des* 136(5):051007
13. Jiao Y, Chawla N (2014) Three dimensional modeling of complex heterogeneous materials via statistical microstructural descriptors. *Integ Mat Manuf Innov* 3(1):1–19
14. Chen D, He X, Teng Q, Xu Z, Li Z (2014) Reconstruction of multiphase microstructure based on statistical descriptors. *Physica A: Statistical Mechanics and its Applications* 415:240–250
15. Xu H, Li Y, Brinson C, Chen W (2014) A descriptor-based design methodology for developing heterogeneous microstructural materials system. *J Mechanical Design* 136(5):051007
16. Xu H, Li Y, Brinson C, Chen W (2013) Descriptor-based methodology for designing heterogeneous microstructural materials system. In: *ASME 2013 International Design Engineering Technical Conferences and Computers and Information in Engineering Conference*. American Society of Mechanical Engineers. pp V03AT03A049–V03AT03A049
17. Ferris KF, Peurrung LM, Marder JM (2007) Materials informatics: fast track to new materials. *Advan Mater Processes* 165(1):50–51, 165(PNNL-SA-52427)
18. Wei Q, Peng X, Liu X, Xie W (2006) Materials informatics and study on its further development. *Chinese Sci Bulletin* 51(4):498–504
19. Sundararaghavan V, Zabarav N (2005) Classification and reconstruction of three-dimensional microstructures using support vector machines. *Comput Mater Sci* 32(2):223–239
20. Basanta D, Miodownik MA, Holm EA, Bentley PJ (2005) Using genetic algorithms to evolve three-dimensional microstructures from two-dimensional micrographs. *Metall Mater Trans A* 36(7):1643–1652
21. Xu H, Liu R, Choudhary A, Chen W (2015) A machine learning-based design representation method for designing heterogeneous microstructures. *J Mechanic Design* 137(5):051403
22. Bai X, Sun C, Zhou F (2008) Touching cells splitting by using concave points and ellipse fitting., pp 271–278
23. Vinzi VE, Trinchera L, Amato S (2010) PLS path modeling: from foundations to recent developments and open issues for model assessment and improvement. In: *Handbook of partial least squares*, Springer Berlin Heidelberg, pp 47–82
24. Goldstein J, Newbury DE, Echlin P, Joy DC, Romig Jr AD, Lyman CE, Lifshin E (2012) *Scanning electron microscopy and X-ray microanalysis: a text for biologists, materials scientists, and geologists*. Springer Science & Business Media, New York, Philadelphia, USA
25. Williams DB, Carter CB (1996) *The transmission electron microscope*. Springer, US, p 3-17

26. Forsyth DA, Ponce J (2002) *Computer vision: a modern approach*, Prentice Hall Professional Technical Reference, New Jersey, USA
27. Morisita M (1962) I σ -Index, a measure of dispersion of individuals. *Res Popul Ecol* 4(1):1–7
28. Xu H, Greene MS, Deng H, Dikin D, Brinson C, Liu W K, Chen W (2013) Stochastic reassembly strategy for managing information complexity in heterogeneous materials analysis and design. *J Mech Des* 135(10):101010
29. Khare HS, Burris DL (2010) A quantitative method for measuring nanocomposite dispersion. *Polymer* 51(3):719–729
30. Luo ZP, Koo JH (2007) Quantifying the dispersion of mixture microstructures. *J Microsc* 225(2):118–125
31. Loehlin JC (1998) *Latent variable models: an introduction to factor, path, and structural analysis*, Lawrence Erlbaum Associates Publishers, New Jersey, USA
32. Thompson B (2004) *Exploratory and confirmatory factor analysis: understanding concepts and applications*, American Psychological Association, Washington, DC, USA
33. Tenenhaus M, Vinzi VE, Chatelin YM, Lauro C (2005) PLS path modeling. *Computational statistics & data analysis* 48(1):159–205.
34. Hair JF Jr, Hult GTM, Ringle C, Sarstedt M (2013) *A primer on partial least squares structural equation modeling (PLS-SEM)*. Sage Publications. California, USA
35. Hair JF, Sarstedt M, Ringle CM, Mena JA (2012) An assessment of the use of partial least squares structural equation modeling in marketing research. *J Acad Marketing Sci* 40(3):414–433
36. Chin WW (1998) The partial least squares approach to structural equation modeling. *Modern Methods Bus Res* 295(2):295–336
37. Debye P, Anderson HR Jr, Brumberger H (1957) Scattering by an inhomogeneous solid. II. The correlation function and its application. *J Appl Phys* 28(6):679–683
38. Lee SY (1990) Covariance structure analysis. *Structural Equation Modeling: A Bayesian Approach*, pp 31–66
39. Wold S, Martens H, Wold H (1983) The multivariate calibration problem in chemistry solved by the PLS method, in *Matrix pencils*, Springer, pp 286–293
40. Fornell C, Bookstein FL (1982) Two structural equation models: LISREL and PLS applied to consumer exit-voice theory. *J Marketing research* 19:440–452
41. Kock N (2013) *WarpPLS 4.0 user manual*. ScriptWarp Systems, Laredo
42. Jin R, Chen W, Sudjianto A (2005) An efficient algorithm for constructing optimal design of computer experiments. *J Stat Plan Inference* 134(1):268–287
43. Stein ML (1999) *Interpolation of spatial data: some theory for Kriging*, Springer-Verlag, New York
44. Huang Y, Krentz TM, Nelson JK, Schadler LS, Li Y, Zhao H, Breneman CM (2014) Prediction of interface dielectric relaxations in bimodal brush functionalized epoxy nanodielectrics by finite element analysis method. In *Electrical Insulation and Dielectric Phenomena (CEIDP)*, 2014 IEEE Conference on. IEEE pp 748-751
45. Kaiser HF (1960) The application of electronic computers to factor analysis, *Educational and psychological measurement*
46. Raïche G et al. (2013) Non-graphical solutions for Cattell's scree test. *Methodology* 9(1):23
47. Horn JL (1965) A rationale and test for the number of factors in factor analysis. *Psychometrika* 30(2):179–185
48. Norris M, Lecavalier L (2010) Evaluating the use of exploratory factor analysis in developmental disability psychological research. *J Autism Dev Disord* 40(1):8–20
49. Hofmann RJ (1978) Complexity and simplicity as objective indices descriptive of factor solutions. *Multivariate Behav Res* 13(2):247–250
50. Roy M, Nelson JK, MacCrone RK, Schadler LS, Reed CW, Keefe R (2005) Polymer nanocomposite dielectrics-the role of the interface. *Dielectrics and Electrical Insulation*, IEEE Transactions on, 12(4):629-643.
51. Ganesh VV, Chawla N (2005) Effect of particle orientation anisotropy on the tensile behavior of metal matrix composites: experiments and micro structure-based simulation. *Mater Sci Eng a-Structural Materials Properties Microstructure Processing* 391(1-2):342–353
52. Thomas M, Boyard N, Perez L, Jarry Y, Delaunay D (2008) Representative volume element of anisotropic unidirectional carbon-epoxy composite with high-fibre volume fraction. *Composites Sci Technol* 68(15):3184–3192
53. Kenney B, Valdmanis M, Baker C, Pharoah JG, Karan K (2009) Computation of TPB length, surface area and pore size from numerical reconstruction of composite solid oxide fuel cell electrodes. *J Power Sources* 189(2):1051–1059
54. Morozov IA, Lauke B, Heinrich G (2011) A novel method of quantitative characterization of filled rubber structures by AFM. *Kgk-Kautschuk Gummi Kunststoffe* 64(1-2):24–27
55. Prakash CP, Mytri VD, Hiremath PS (2010) Classification of Cast Iron Based on Graphite Grain Morphology using Neural Network Approach. *Second International Conference on Digital Image Processing*, International Society for Optics and Photonics, pp 75462S–75462S
56. Klayson C, Moon SH, Ladewig BP, Lu GM, Wang L (2011) The effects of aspect ratio of inorganic fillers on the structure and property of composite ion-exchange membranes. *J Colloid Interface Sci* 363(2):431–439
57. Jean A, Jeulin D, Forest S, Cantournet S, N'GUYEN F (2011) A multiscale microstructure model of carbon black distribution in rubber. *J Microsc* 241(3):243–260